ELSEVIER

Catalysis Today 49 (1999) 467–484

CATALYSIS TODAY

The origin of the support effect in supported metal oxide catalysts: in situ infrared and kinetic studies during methanol oxidation

Loyd J. Burcham, Israel E. Wachs*

Department of Chemical Engineering and Zettlemoyer Center for Surface Studies, Lehigh University, Bethlehem, PA 18015, USA

Abstract

The strong influence of the oxide support upon the turn-over frequency (TOF) of methanol oxidation over supported metal oxide catalysts has been well documented in recent years. However, the mechanistic origins (adsorption equilibrium of methanol to methoxy species, rate-determining methoxy surface decomposition, or product desorption equilibrium) of this interesting phenomenon are not completely understood. In order to obtain additional insight, the steady-state surface concentrations of adsorbed methoxy intermediates on monolayer catalysts ($\sim$8 V atoms nm^{-2}) of V_2O_5/(TiO_2, CeO_2, Al_2O_3 and ZrO_2) have been quantified with in situ transmission infrared spectroscopy/mass spectrometry. Calculations of the adsorption equilibrium constant, K_{ads}, show a $\sim$ six times increase for vanadia on oxide supports of Al < Ti < Zr < Ce, whereas the methoxy surface decomposition rate constant, k_{rds} (rds = rate-determining step), shows a $\sim$ 22 times increase in value over these same catalysts. Thus, changes in both the adsorption equilibrium and the methoxy decomposition properties of supported metal oxide catalysts appear to be responsible for the support effect, although the methoxy decomposition is clearly the reaction step that is more sensitive to the specific metal oxide support. More fundamentally, the support effect appears to correlate with the electronegativity of the support cation, which is proposed to have influence upon the rate of methoxy decomposition through hydride abstraction and on the steady-state equilibrium adsorption capacity of methanol to surface methoxy intermediates through the basicity of the bridging V–O–support bond (the adsorption site).

1. Introduction

The selective oxidation of methanol to formaldehyde is commercially important for the production of valuable phenolic resins and the catalysts employed industrially are typically unsupported $Fe_2(MoO_4)_3$–MoO_3 mixtures or silver [1,2]. However, high activities and selectivities for this reaction have also been well documented in supported metal oxide catalysts, in which the active metal oxide is molecularly dispersed as a two-dimensional metal oxide overlayer on a high surface area support oxide [3]. In particular, catalysts with vanadia and molybdena supported on alumina and titania (and less frequently on ceria, zirconia, silica and niobia) are among the most well studied of this type of catalyst [2–9,11–14]. Unlike the bulk oxide catalysts used industrially, these supported metal oxide materials can serve as model catalysts for a number of reasons. First, the number of active sites and the ratio of isolated/polymerized species may be controlled by varying the loading of the active metal oxide since the active oxide is 100% dispersed on the support below monolayer coverage. Second, the influence of the M–O–support interaction (M = V, Mo, or

*Corresponding author. Tel.: +1-610-7586555.

0920-5861/99/$ – see front matter
PII: S0920-5861(98)00442-8

other active surface metal oxide) can be monitored by changing the specific support ligand (Al, Ti, Ce, etc.) upon which the active metal oxide species is anchored (the nature of the active site can also be affected by varying the surface promoter neighbors). Third, molecular structural information about the active site can be obtained with in situ spectroscopies (e.g., IR, Raman and UV–Vis DRS), often without being complicated by overlapping signals from the underlying support oxide.

Previous reactivity studies of these supported metal oxide model catalysts have indicated a strong support effect upon the turn-over frequency (TOF) of the methanol oxidation reaction [3,4,6–11]. This is best illustrated with supported vanadia catalysts since a large amount of research has been performed on these catalytic systems [3,4,6–9,19]. The TOF over supported vanadia catalysts is defined as the number of methanol molecules converted to formaldehyde per surface V atom per second. Monolayer coverage, determined experimentally as the highest loading of vanadia that does not generate bulk V_2O_5 crystal bands in the Raman spectrum, corresponds to 3 wt.% vanadia on ceria (36 $m^2\,g^{-1}$; 5.7 V atoms nm^{-2}), 4% on zirconia (39 $m^2\,g^{-1}$; 6.8 V atoms nm^{-2}), 5% on titania (55 $m^2\,g^{-1}$; 7.9 V atoms nm^{-2}) and 25% on alumina (250 $m^2\,g^{-1}$; 7.3 V atoms nm^{-2}) [8,9]. Under 6% methanol, the TOFs for catalysts at monolayer coverages were found to be highest for vanadia on ceria ($1.0 \times 10^{+0}\,s^{-1}$), followed by V_2O_5/ZrO_2 ($1.7 \times 10^{-1}\,s^{-1}$) and V_2O_5/TiO_2 ($1.1 \times 10^{-1}\,s^{-1}$) and was much lower for V_2O_5/Al_2O_3 ($6.8 \times 10^{-3}\,s^{-1}$) [8,9]. However, the origin of this support effect on TOF is not completely understood at present. A deeper fundamental understanding of this effect requires that structure–reactivity relationships be developed for the individual reaction steps (adsorption, surface reaction and desorption) involved in the overall methanol oxidation reaction.

Molecular structural information about the active surface vanadia sites on calcined, dehydrated catalysts has been obtained by Raman, IR, UV–Vis DRS, ^{51}V solid state NMR, EXAFS/XANES and $^{18}O_2/^{16}O_2$ exchange experiments [3,4,6–9]. These molecular characterization techniques have demonstrated that the active site is a VO_4 unit possessing a single V=O (mono-oxo) terminal bond, three bridging V–O–M bonds (M = V or support cation) and that the

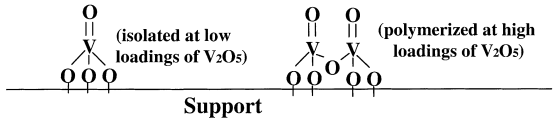

Fig. 1. Schematic drawing of the surface vanadia species (note that polymers may be very long).

vanadium atom is in the +5 oxidation state after calcination. Both isolated and polymerized VO_4 units exist on the surface, the ratio of polymerized to isolated surface vanadia species increasing with increasing surface coverage [7]. The surface vanadia structure is essentially the same on all of the supports studied (CeO_2, ZrO_2, TiO_2 and Al_2O_3), except for very small differences in the bond length of the terminal V=O bond (±0.01 Å). The density of active vanadia surface sites is also the same on all of the supports at monolayer coverage (~8 V atoms nm^{-2}). A schematic drawing of the surface vanadia structure is given in Fig. 1.

In situ Raman spectroscopy measurements have shown that the relative percent reduction of V^{+5} species during methanol oxidation, and hence the fraction of vanadia sites which are active during the steady-state reaction, are roughly the same on all of the vanadia monolayer catalysts [7]. The absolute extent of reduction cannot be determined from the in situ Raman spectra because the Raman scattering cross-sections are highly non-linear with concentration, but recent in situ UV–Vis DRS spectra indicate very little reduction during reaction (~10% decrease in V^{+5} band intensity) [15]. Furthermore, oxygen isotope exchange experiments coupled with Raman spectroscopy suggest that the V=O bond exchanges oxygen isotopes at rates much slower than the reaction rate and therefore implicate the V–O–support bonds as the critical redox centers. Thus, from a structural viewpoint, the support effect appears to originate from differences in the bridging V–O–support bond as the support is varied and may be related to the electronegativity of the support cation [8,9]. However, the relationship between this structural observation and the specific reaction steps in the methanol oxidation mechanism is not well understood. More precisely, which mechanistic step (adsorption, surface decomposition, or desorption) does the structural support effect most significantly relate to during reaction?

When this question is answered, a true structure–reactivity relationship will be obtained that fully explains the support effect (i.e, from both a molecular structural and reactivity point of view).

The overall kinetics of methanol oxidation to formaldehyde are fairly well described [16–19], the stoichiometry of the reaction being given as follows:

$$CH_3OH + \frac{1}{2}O_2 = CH_2O + H_2O \quad (1)$$

Furthermore, the catalytic surface reaction follows a mechanism similar to the Mars–Van Krevelen pathway, in which the methanol dissociatively chemisorbs as a surface methoxy intermediate and a surface hydroxyl on an active site. The surface methoxy intermediate subsequently decomposes into gas-phase formaldehyde and another surface hydroxyl. The surface hydroxyls then recombine and desorb as water, while the catalyst is reoxidized by a 'pool' of adsorbed oxygen atoms supplied by excess oxygen in the gas phase. The mechanism is summarized as follows (S = support cation):

$$CH_3OH + V{-}O{-}S \leftrightarrow CH_3O{-}V + S{-}O{-}H \quad (2)$$

$$CH_3O{-}V + O_{ads} \rightarrow CH_2O + V{-}OH \quad (3)$$

$$S{-}OH + V{-}O{-}H \leftrightarrow H_2O + V{-}O{-}S \quad (4)$$

At low conversions, the selectivity to formaldehyde is 90–99% over 5% V_2O_5/TiO_2, 3% V_2O_5/CeO_2 and 4% V_2O_5/ZrO_2, but only about 50% selective over 25% V_2O_5/Al_2O_3 due to the presence of surface Lewis acid sites on alumina [6,8,9]. Non-selective side reactions include readsorption of formaldehyde as formate species, which decompose to CO and CO_2, as well as acidic reactions on V_2O_5/Al_2O_3 to form dimethyl ether [6,8,9,11].

Kinetic isotope studies have shown that the surface decomposition of the adsorbed methoxy intermediate is rate determining [16]. Therefore, the rate of the overall reaction is derived from Eq. (3) as follows:

$$TOF = k_{rds} \times \theta_{OCH_3} \quad (5)$$

where k_{rds} is the rate constant for the rate-determining surface decomposition of surface methoxy to formaldehyde and θ_{OCH_3} is the fractional surface coverage of adsorbed methoxy intermediates (in methoxy molecules per surface vanadium atom). Holstein and Machiels [16] have derived from the mechanism given in Eqs. (2)–(4) the expression for θ_{OCH_3} in terms of gas-phase species (in the presence of excess oxygen and assuming a fully oxidized surface with low surface methoxy coverage – in which case the Langmuir isotherm reduces to a simple proportionality):

$$\theta_{OCH_3} = \frac{K_1 \frac{P_{CH_3OH}}{\frac{1}{P_{H_2O}^2}}}{\frac{1}{K_2^2}} \quad (6)$$

where K_1 and K_2 are the adsorption equilibrium constants for steps (2) and (4), respectively, and P_{CH_3OH} and P_{H_2O} are gas-phase partial pressures. When Eq. (6) is substituted into Eq. (5), the overall rate expression is obtained:

$$TOF = \frac{k_{rds}K_1 \frac{P_{CH_3OH}}{\frac{1}{P_{H_2O}^2}}}{\frac{1}{K_2^2}} \quad (7)$$

The first-order dependence of the rate on methanol concentration and the negative one-half order dependence on water is also empirically verified [16]. A simplification can be made for single-pass reactors at low methanol conversions (below 10%) without water in the feed stream, in which the water dependence is pseudo zero-order. Under these conditions, the expression for the overall rate of reaction becomes:

$$TOF = k_{overall} \times P_{CH_3OH}, \quad \text{where } k_{overall} = K_{ads} \times k_{rds} \quad (8)$$

Eq. (8) must be used with caution, however, as product inhibition by water will affect the reaction rate at higher conversions or in multi-pass recycling reactors [16]. If water inhibition does become significant then the apparent methanol reaction order in Eq. (8) becomes 2/3 instead of 1 and the $k_{overall}$ constant becomes falsified unless Eq. (7) is used to account for the water inhibition [16]. Nevertheless, Deo and Wachs [6] have shown that Eq. (8) is valid under the moisture-free differential conditions described above. They calculated methanol oxidation activation energies over supported vanadia catalysts in a moisture-free single-pass PFR to be ~20 kcal mol^{-1} – the same value obtained by Holstein and Machiels [16] in a water inhibited multi-pass reactor when the inhibition is taken into account. This value is also the activation energy for C–H bond breaking in adsorbed methoxy species, which is consistent with step (3) being the rate

determining step in heterogeneous catalytic methanol oxidation [16]. The close agreement between the methanol oxidation activation energy and the known activation energy for C–H bond breaking in methoxy species also suggests that the heat of methanol adsorption has a relatively small magnitude, since a significant heat of adsorption (usually negative in sign) would have lowered the apparent activation energy ($E_{app} = E_a + \Delta H_{ads}$) [8,9,16].

Although the surface decomposition is the rate-determining step, it may not be responsible for the orders of magnitude differences observed in the TOF between different supported vanadia catalysts. Specifically, temperature programmed reaction spectroscopy (TPRS) studies, which are sensitive to the rate of the surface decomposition as all of the adsorption steps occur before initiating the reactive temperature ramp, indicate a peak temperature, T_p, for the production of CH_2O at about 210°C for all of the monolayer vanadia catalysts studied [8,9]. This constant TPRS peak temperature suggests that the actual rate constant for the rate-determining step k_{rds} in Eq. (5), is roughly constant for all of the monolayer vanadia catalysts [8,9]. Therefore, differences in the adsorption equilibria and hence in the steady-state concentration of methoxy intermediates, θ_{OCH_3} in Eq. (5), may be responsible for the significant differences in TOF.

However, more recent TPRS studies have revealed different desorption peak temperatures for vanadia on alumina ($T_p \approx 210$°C) versus vanadia on titania ($T_p \approx 180$°C) when the initial adsorption occurs at room temperature (the original TPRS studies adsorbed methanol at 100°C) [20]. This contradictory behavior between the TPRS peak temperatures is probably caused by different extents of surface reduction on the catalysts after methanol adsorption. Such reduction can only occur by some small amount of methoxy surface decomposition as the adsorption itself is non-reducing, and reduction after adsorption at 100°C is likely to reduce the catalysts more than adsorption at room temperature. Consequently, the catalysts are not fully oxidized, or even reduced to the same extent, when beginning the reactive temperature ramp at 100°C that eventually leads to a desorption peak. The individual reaction step responsible for the support effect may not be adsorption alone, as suggested by the initial TPRS data, because another important parameter – the oxidation state of vanadium atoms – is also complicating the TPRS results.

The purpose of the present study is to better determine the origin of the support effect in supported metal oxide catalysts by directly measuring the steady-state concentrations of surface methoxy intermediates with in situ infrared spectroscopy, since IR can easily detect adsorbed organic surface species. The relative significance of the adsorption and surface decomposition steps toward the support effect will then be ascertained from these measurements. Monolayer coverages were chosen for the various catalytic systems as they minimize the amount of exposed adsorption sites on the bare support, which produce stable spectator methoxy species rather than reactive intermediates. Also, mass transfer effects in the IR experiments are important and will be discussed when appropriate.

2. Experimental

The catalysts used in this study were prepared by the incipient wetness impregnation method. This technique is described in detail elsewhere [6,8,9], so only a brief summary is given here. The supports (γ-Al_2O_3 with 250 $m^2\,g^{-1}$ from Engelhard; P-25 TiO_2 with 55 $m^2\,g^{-1}$ from Degussa; CeO_2 with 36 $m^2\,g^{-1}$ from Engelhard; and ZrO_2 with 39 $m^2\,g^{-1}$ from Degussa) were first calcined to 723–773 K and then cooled to room temperature. The supports were then impregnated with solutions of vanadium triisopropoxide (Alfa, 98% pure) and methanol (Fisher-certified ACS, 99.9% pure) under a nitrogen atmosphere inside a glove box. After thorough mixing, the samples were dried at room temperature in the glove box for 16 h, followed by heating to 393 K under nitrogen. Finally, the samples were calcined to 723 K (TiO_2, CeO_2 and ZrO_2 samples) and 773 K (Al_2O_3 samples) in pure oxygen (Linde, 99.99% pure) for 4 h. The differences in calcination temperature were designed to prevent sintering of the less thermally stable TiO_2, CeO_2 and ZrO_2 supports.

The in situ infrared/mass spectrometer experiments were performed with a BioRad FTS-40A FTIR Spectrometer coupled to a Fissions Quadropole Mass Spectrometer. The infrared spectra were recorded at a resolution of 2 cm^{-1} using 250 signal-averaged

scans and, after acquisition, were smoothed using the Savitsky–Golay method (20-point, second-degree polynomial). The IR was operated in transmission mode using a specially designed in situ cell, which is described below. Transmission mode was selected for this work to take advantage of the linear absorbance signal dictated by Beer's Law and due to the inherent difficulties involved in quantitative reflectance methods such as DRIFTS (diffuse reflectance) and ATR (attenuated total reflectance). Calibration of the methoxy IR signal was achieved by quantitatively dosing known amounts of methanol onto the catalysts at 110°C under vacuum (a special vacuum system for volumetric dosing was designed and constructed for this purpose). The IR signal was detected with a DTGS detector and the mass spectrometer utilized a Faraday detector. Also, gas lines between the cell exit and the mass spectrometer detection chamber were kept as short as possible and were heated to 120–130°C to prevent polymerization and condensation of the formaldehyde produced by the reaction. These experimental systems are schematically shown in Fig. 2.

The infrared transmission cell was specially designed to provide a minimum of dead space during in situ experiments. The design, made entirely of 316 stainless steel, is also illustrated schematically in Fig. 2, where it can be seen that the cell is essentially a straight tube with gas inlet and outlet ports located as close to the KBr windows as possible. The sample is placed normal to the gas flow direction into a small groove (0.025″) made in the center of another, smaller diameter tube of the same length as the outer tube. The sample diameter exposed to the IR beam when the wafer is placed in this groove is 10 mm. The smaller tube is then inserted, with the sample, into the larger tube until the sample rests against a thermocouple well in the center of the larger tube. The 32 mm KBr windows are affixed by 1″ VCO® O-ring fittings (Cajon). The O-rings are made of Viton® and are, therefore, thermally stable to 204°C. This method of window attachment has the advantage of easy removal for sample replacement, thermal stability, and it is leak free from high vacuum to several atmospheres using only a finger-tight force on the VCO nut. The center of the tube is heated with standard heavy insulated heating tape and 1/8 in. copper tubing is wrapped around the ends of the cell to provide water cooling for the Viton® O-rings and KBr windows.

The residence time of the in situ IR cell was measured by room temperature tracer experiments,

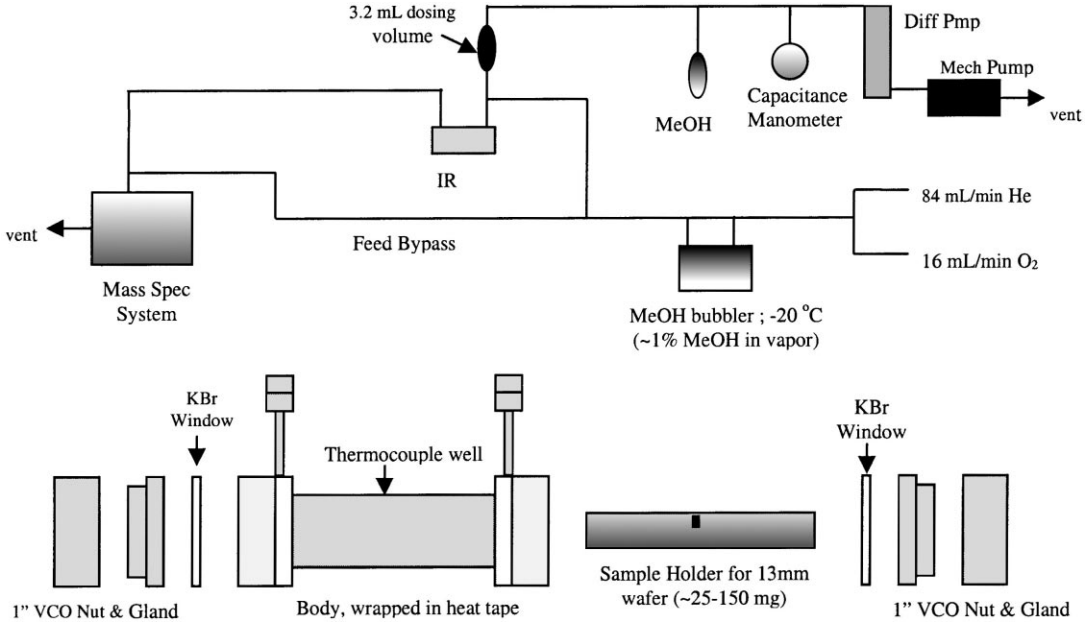

Fig. 2. Experimental apparatus.

in which 5 ml pulses of air were injected, with a syringe, through a septum into a He gas stream. The O_2 signal (mass 32) was then measured as a function of time with the mass spectrometer. There was relatively little broadening of the pulse as it traveled through the empty cell and addition of an Al_2O_3 wafer did not cause any further broadening. Therefore, it may be assumed that the cell has very little holdup due to backmixing (<20 s residence time as measured by these tracer experiments).

The following experimental procedure was employed. Samples of ~30–60 mg were first pressed (using about 4 t of force on a 1/2 in. die, or ~40 000 psi) into self-supporting catalyst wafers that were thin enough (~0.1 mm thick; 13 mm diameter) that significant IR transmission was possible. After being weighed and loaded into the IR cell, the samples were heated in situ to 325°C in flowing oxygen (16 ml min^{-1}; ultra high purity; JWS Technologies) and helium (84 ml min^{-1}; ultra high purity; JWS Technologies). The pretreated catalysts were then cooled to 100°C and methanol (semiconductor grade; Fisher Scientific) was introduced at about 1.15% concentration by bubbling the gas through a methanol bubbler. This low concentration of gas-phase methanol, which was necessary in order to reduce gas-phase methanol signals in the in situ IR experiments, was obtained by holding the bubbler at −20°C in a recirculating bath of water and ethylene glycol. The temperature was then slowly ramped to 200°C, 225°C, 250°C, 275°C and 300°C under an O_2/He/CH_3OH flow (15 : 84 : 1 ratio to ensure oxidizing conditions).

IR and mass spectra were obtained at each temperature after the signals had reached stable, steady-state values. Additionally, a feed bypass allowed for mass spectra to be taken at each temperature immediately after recording the signal from the cell exit, thus accounting for any variations in the feed composition during the experiment. The gas-phase compositions were recorded by the mass spectrometer using a leak valve set to maintain 3.0×10^{-6} Torr of total pressure in the detection chamber. Masses 18, 31 and 44 were used to monitor water, methanol and CO_2, respectively, since these ion fragments originate predominantly from their respectively indicated species without significant overlap. Mass 29 was used to monitor formaldehyde, but subtraction of the methanol fragment contribution at this mass was also required. This was accomplished using the mass 29/31 fragmentation ratio of methanol obtained from the feed mass spectrum (where no formaldehyde was present). Also, blank runs using the empty cell in the standard experimental procedure resulted in no detectable conversion of methanol, even up to 300°C, demonstrating that the low surface area stainless steel does not contribute to the measured catalytic data.

3. Results

3.1. Steady state, in situ IR spectra

The results of the in situ IR/mass-spectrometer methanol oxidation studies ($100°C > T < 300°C$ in flowing O_2/He/CH_3OH) are given in Figs. 3–6. Surface structural information about the catalysts can be obtained from the IR band positions and intensities of the VO_4 units that comprise the surface active sites during methanol oxidation. Unfortunately, the catalyst supports (Al_2O_3, TiO_2, and ZrO_2) are highly absorbing in the IR region around the fundamental symmetric stretching vibration of these VO_4 units (dominated by the V=O mono-oxo stretch at ~1030 cm^{-1} [21]). Vuurman et al. [21] have identified these fundamentals as weak shoulders in the transmission spectra of very thin wafers, but generally these vibrations are obscured by the support. A very interesting exception is the 3% V_2O_5/CeO_2 catalyst, which exhibits a sharp V=O symmetric stretching band at 1029 cm^{-1} (with shoulders at 1034 and 1023 cm^{-1}) as the CeO_2 support is only weakly absorbing in this IR region (see Figs. 5 and 7). The 3% V_2O_5/CeO_2 catalyst also exhibits an IR band at ~927 cm^{-1}, which similarly appears in the Raman spectrum [22] and is assigned to V–O–V polymer stretching vibrations. All of the catalysts exhibit very weak V=O stretching overtones around 2040 cm^{-1}, as well, but these overtone signals are lost within the experimental noise upon adsorption of methanol and cannot provide in situ structural information.

The presence of strong V=O stretching bands in Fig. 7 for the 3% V_2O_5/CeO_2 catalyst offers a unique opportunity to study the structural behavior of this supported metal oxide catalyst under in situ conditions. Jehng et al. [22] also found that the 3% V_2O_5/CeO_2 catalyst exhibits a broad Raman band (centered

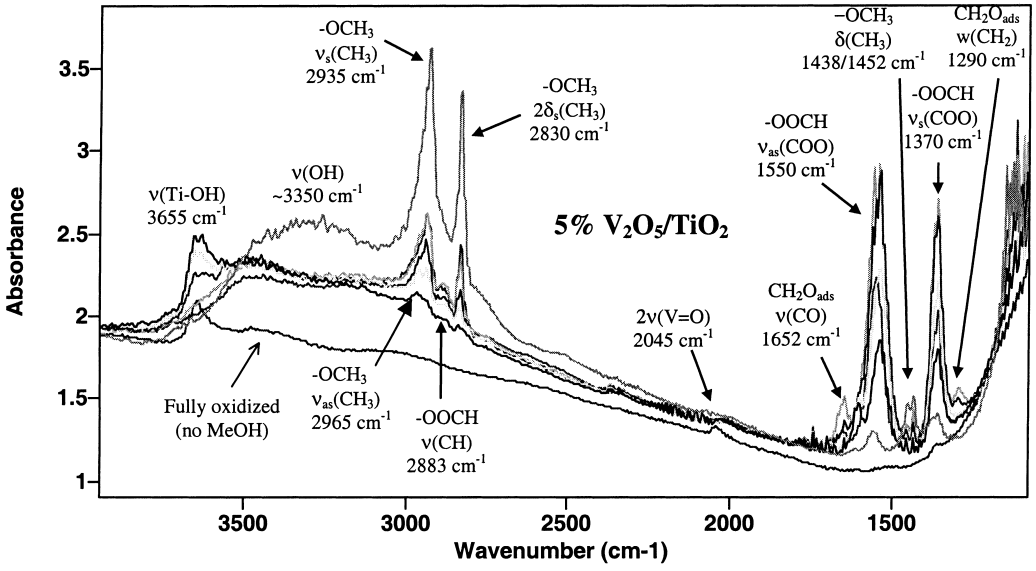

Fig. 3. In situ IR spectra of 5% V_2O_5/TiO_2 during methanol oxidation as a function of temperature (lowest temperatures on top; 100°C, 200°C, 225°C, 250°C, 275°C and 300°C). Note: bands for physisorbed water (1615 cm^{-1}) and physisorbed methanol (2850, 2955 and 1370 cm^{-1}) are too weak to be observed in these spectra.

at ~1026 cm^{-1}) corresponding to the V=O symmetric stretching vibration. The presence of Raman shoulders are indicated, as well, and the multiple IR and Raman V=O bands might seem to indicate multiple V=O stretching modes within the same VO_4 unit (i.e., a di-oxo species like O=V=O). However, a di-oxo species would be expected to have two bands in each spectrum – the symmetric stretch being more intense

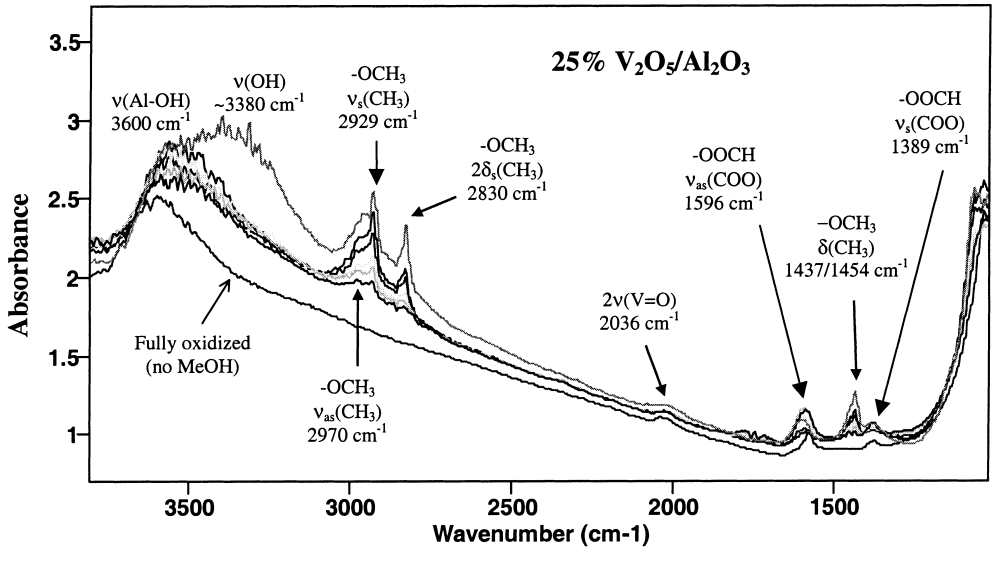

Fig. 4. In situ IR spectra of 25% V_2O_5/Al_2O_3 during methanol oxidation as a function of temperature (lowest temperatures on top; 100°C, 200°C, 225°C, 250°C, 275°C and 300°C). Note: at the lowest temperature (100°C), a weak shoulder at 2956 cm^{-1} indicates the presence of some physisorbed methanol.

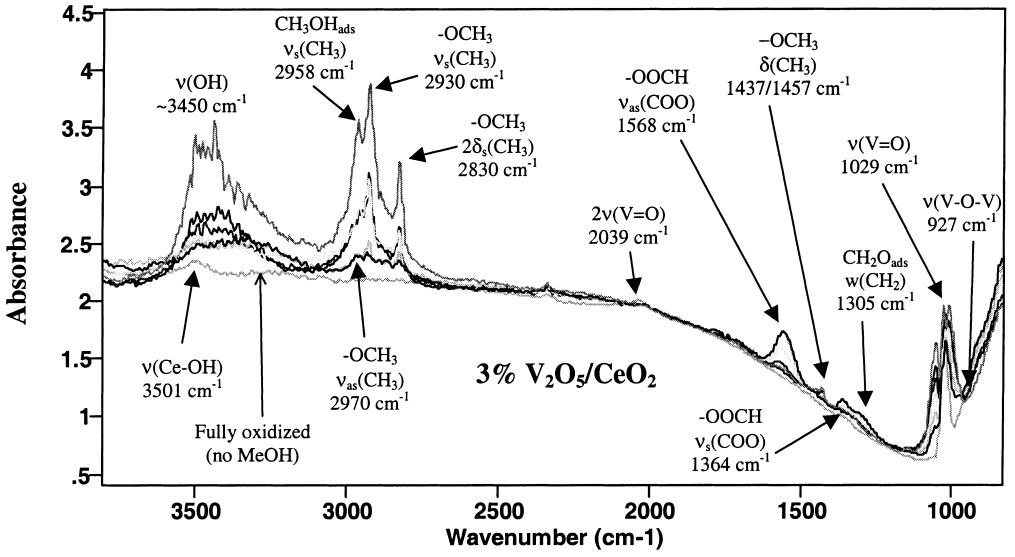

Fig. 5. In situ IR spectra of 3% V_2O_5/CeO_2 during methanol oxidation as a function of temperature (lowest temperatures on top; 100°C, 200°C, 225°C, 250°C, 275°C and 300°C). Note: gas-phase methanol has bands at 1014, 1034 and 1058 cm^{-1}, appearing as shoulders on the V=O stretching band at 1029 cm^{-1}.

in Raman and the asymmetric stretch being more intense in IR. The correspondence between the IR ($\sim$1029 cm^{-1}) and Raman ($\sim$1026 cm^{-1}) V=O stretching modes suggests, instead, that the shoulders correspond to V=O mono-oxo species within VO_4 units of slightly different symmetry (i.e., isolated and polymerized species). In principle, the decrease in IR absorption intensity during in situ methanol

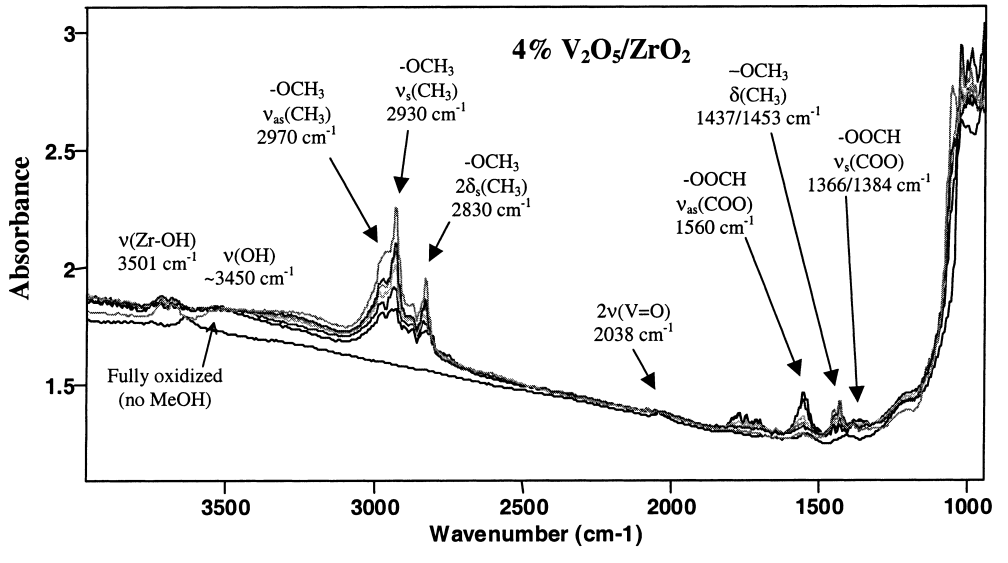

Fig. 6. In situ IR spectra of 4% V_2O_5/ZrO_2 during methanol oxidation as a function of temperature (lowest temperatures on top; 100°C, 200°C, 225°C, 250°C, 275°C and 300°C).

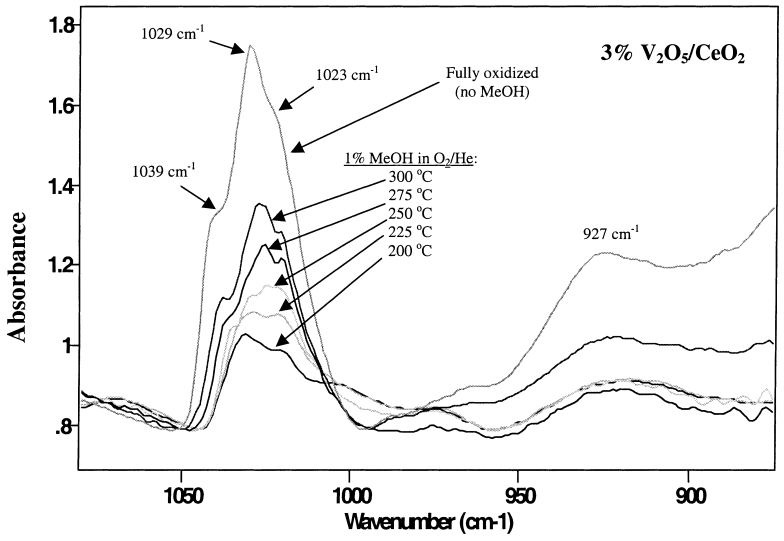

Fig. 7. V=O fundamental region in 3% V_2O_5/CeO_2. Note: methanol bands have been subtracted from the spectra obtained during in situ methanol oxidation.

oxidation experiments could also provide information about the percent reduction of the catalyst during reaction. However, below 300°C the vibrational modes of the catalyst V=O bonds have been shown to be significantly perturbed by hydrogen bonding with water, methanol, and organic surface species [22]. At reaction temperatures (200–300°C), this means that the infrared extinction coefficients for the V=O stretch are not likely to be constant as the temperature and, hence, the steady-state concentration of surface methoxy intermediates are changed. At 300°C, where these effects are minimized but not eliminated, a 24% decrease is observed in the integrated intensity of the V=O band at 1029 cm^{-1}, relative to its undistorted value, and this implies that most of the vanadia sites are in the fully-oxidized V^{+5} state during methanol oxidation.

For quantification of adsorbed surface methoxy species (which do follow Beer's Law; see detailed discussion below for the calibration methods), recall that the catalysts used for these studies were 25 wt.% V_2O_5/Al_2O_3, 5% V_2O_5/TiO_2, 3% V_2O_5/CeO_2, and 4% V_2O_5/ZrO_2. These vanadia loadings correspond to monolayer coverage (~8 V atoms nm^{-2}), and were chosen in order to limit the number of bare support sites on the catalyst surface – such sites can lead to the adsorption of undesired spectator methoxy species that remain stable until ~300°C before decomposing into CO/CO_2 and water. The presence of such spectators would complicate the IR spectra, although the band positions for surface methoxy vibrations are usually dependent upon the specific ligand and, hence, the unreactive support–methoxy species could probably be distinguished from the reactive vanadium–methoxy species [14].

The IR spectra given in Figs. 3–6 exhibit the same vibrational modes for adsorbed surface species as was observed and tabulated previously by Busca et al. [14] for supported vanadia catalysts in non-steady state, vacuum conditions. Following Busca's assignments, the major methoxy (OCH_3) bands in the in situ IR spectra (see labels in Fig. 3) include bands at 2935 and 2830 cm^{-1}, which arise from Fermi resonance between the symmetric stretch and first overtone of the symmetric bend of CH_3 units in adsorbed OCH_3 species, respectively. The unusual intensity of these symmetric stretching bands is attributed to the Fermi resonance occurring between them [14]. The asymmetric stretch of the CH_3 units in adsorbed OCH_3 species occurs as a weaker shoulder around 2965 cm^{-1}. Other methoxy bands include CH_3 bending vibrations at 1452 and 1438 cm^{-1} and a very weak C–O stretching mode at 1150 cm^{-1} [14]. However, these lower frequency methoxy modes are generally weak relative to the nearby formate ($HCOO-$) bands at 1550 cm^{-1} (O–C–O asymmetric stretch) and 1370 cm^{-1} (O–C–O symmetric

stretch). Higher frequency C–H stretching modes for the formate species appear at 2883 and 2975 cm^{-1} but are very weak. Vibrations due to OH groups cause very broad absorbance between 3300 and 3500 cm^{-1}.

Band assignments for physisorbed species [14] include physisorbed water (bending mode at 1615 cm^{-1}), physisorbed formaldehyde (CH_2O_{ads}; bands at 1290 and 1650 cm^{-1}), and physisorbed methanol (CH_3OH_{ads}; bands at 2955, 2850 and 1370 cm^{-1}). In particular, the 2850 cm^{-1} band of CH_3OH_{ads} must be minimized, by lowering the gas-phase methanol concentration, so that the 2830 cm^{-1} surface methoxy band may be integrated. In fact, with the low vapor-phase concentration of 1% methanol used in this study, the only gas-phase methanol bands observed are at 1014, 1034 and 1058 cm^{-1}, and they appear only as shoulders on the V=O stretching band in 3% V_2O_5/CeO_2 (Fig. 5). Finally, the physisorbed water, methanol, and formaldehyde species are minority components with IR bands of relatively weak intensity at all temperatures above 100°C, but the disappearance of the water band (1615 cm^{-1}) at these temperatures is especially important as it supports the assumption of pseudo zero-order P_{H_2O} kinetics.

From the IR data, the relative change in concentration of the surface methoxy intermediates was calculated by integrating the IR band at ~2830 cm^{-1} in the collected spectra. This band has relatively little overlap with other vibrational bands in the spectra and, therefore, provides the best signal for quantitation. Transient experiments (not shown) at 225°C, in which the methanol was suddenly removed from the O_2/He mixture, showed that essentially all of the observed surface methoxy bands were converted within several minutes – often with an increase in formate bands. Hence, the surface methoxy species present on the monolayer catalysts are not spectator species as spectator species would be stable on the surface until well above 300°C before decomposing to CO, CO_2 and H_2O.

3.2. *Determination of extinction coefficient (2830 cm^{-1} band)*

Absolute quantification of the number of surface methoxy species adsorbed per surface vanadium atom, θ_{OCH_3}, required the determination of the extinction coefficient for the 2830 cm^{-1} IR band (i.e., the slope of the calibration curve relating the integrated IR signal of the 2830 cm^{-1} band to μmoles OCH_3 on the surface). This extinction coefficient was determined following the volumetric method described by Emeis [23], in which methanol was quantitatively adsorbed onto the catalyst in steps (~1 μmol methanol in each step) with IR spectra recorded after each stepwise addition. Saturation of the surface with methoxy species is indicated by a leveling off of the signal versus concentration curve due to the formation of physisorbed and gas-phase methanol species. Also, the vacuum pressure begins to increase after surface saturation due to the increasing pressure of gas-phase methanol. The stepwise quantitative adsorption is carried out at 110°C to ensure that the methanol only adsorbs as surface methoxy species (otherwise, the known μmoles of methanol introduced onto the sample will not correspond to the μmoles of surface methoxy species). At lower adsorption temperatures, the methanol will adsorb to form both surface methoxy species and physisorbed methanol, while at higher temperatures the surface methoxy species will react to form formaldehyde.

The results of these dosing experiments showed a high degree of linearity ($r = 0.995$), and the passage of the lines through the origin indicates that methanol adsorption at 110°C on these catalysts produces only surface methoxy species. Adsorption of methanol to other species or on the cell walls would have forced the lines away from the origin and most likely would have generated non-linear calibration curves. The extinction coefficient, therefore, was calculated from the slope of these lines to be 13.3 cm^{-1} per μmole of surface methoxy molecules per gram catalyst (for a 50 mg wafer). Variations in the extinction coefficient between 100°C and 300°C and upon changing the vanadia support are expected to be very small [23]. The methoxy saturation of the 5% V_2O_5/TiO_2 catalyst used in these dosing experiments occurred at about 0.4 surface methoxy molecules per V atom, which is consistent with recent thermogravimetric (TGA) results under similar non-oxidizing, non-steady state conditions [24]. Furthermore, the same saturation value was obtained when the TGA experiment was repeated on compressed IR wafers (instead of the usual 75 micron powders) – indicating that the process of compressing the catalyst powders into thin IR wafers does not affect the microporosity or number

of accessible sites (although diffusion limitations during reaction are still possible in steady-state flow experiments if either the reaction rate or particle size/wafer thickness are large; see Appendix A).

3.3. *Surface methoxy concentrations and CH_3OH oxidation activity data*

The surface methoxy concentrations, normalized to the number of surface vanadium atoms in the samples, are summarized in Fig. 8(a). The integrated intensities and, hence, the steady-state concentrations of surface methoxy intermediates decrease with increasing temperature. This is expected because more surface methoxy species are reacted to CH_2O (k_{rds}) relative to methanol dissociative adsorption (K_{ads}) as the temperature increases (i.e., K_{ads} decreases with temperature, whereas k_{rds} increases with temperature). Also, the values for surface methoxy concentration, θ_{OCH_3}, are all less than one methoxy molecule per V atom.

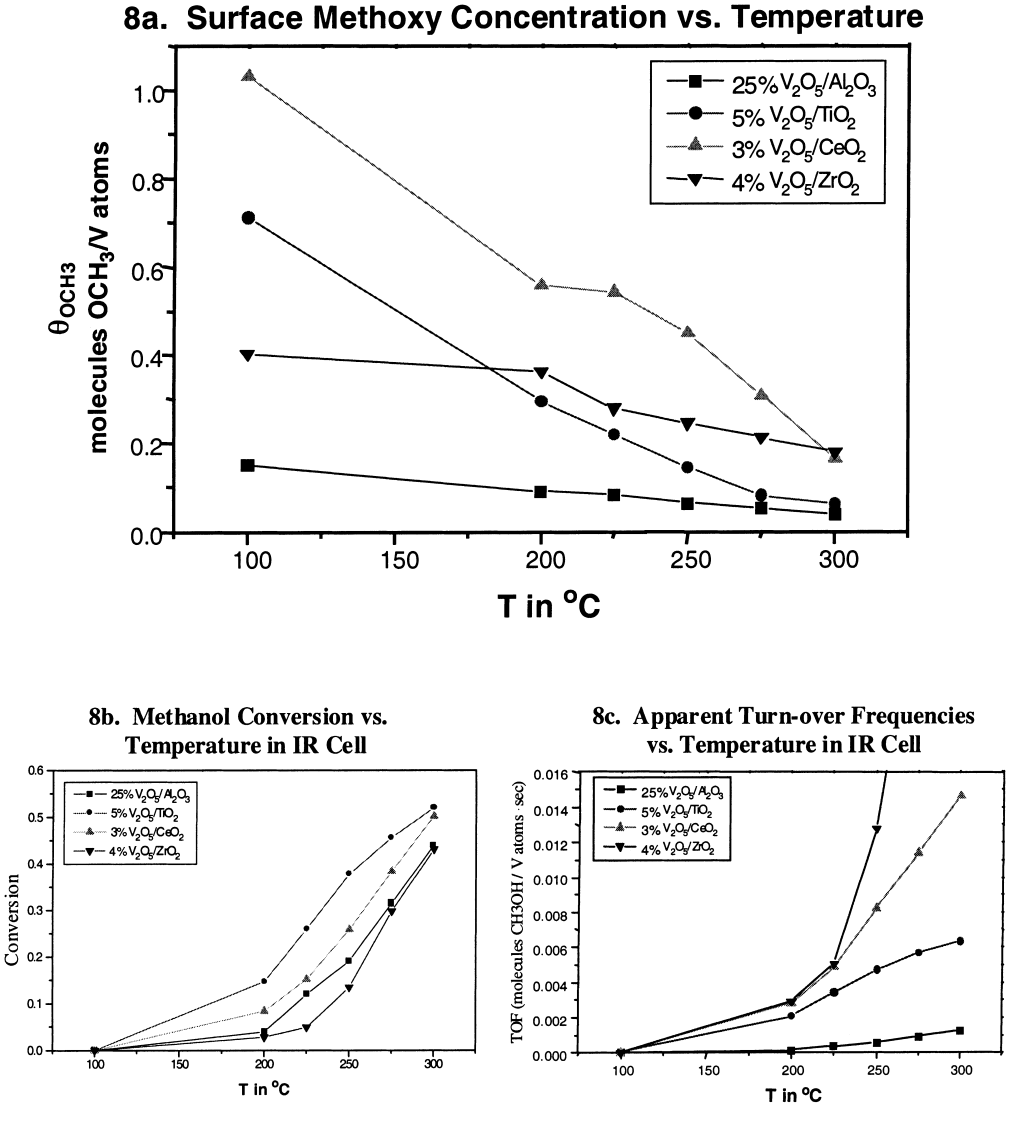

Fig. 8. Summary of IR and mass spectroscopic data.

This indicates that no more than one methanol molecule can dissociatively chemisorb on a VO_4 unit in the formation of a surface methoxy intermediate (assuming that all vanadium atoms are accessible in a two-dimensional oxide monolayer). The fact that some of the steady-state methoxy concentrations, especially those at 100°C, are slightly higher than the 0.4 methoxy molecules per V atom detected at saturation during IR and TGA chemisorption experiments may be related to the higher partial pressures of methanol (1%) used in the steady-state experiments (the TGA experiments were performed at 2000 ppm methanol). Nevertheless, Fig. 8(a) shows that at reaction temperatures (>200°C) even a steady-state flow of 1% methanol produces relatively low surface methoxy concentrations (<0.3 methoxy molecules per V atom for vanadia on Al_2O_3, TiO_2, and ZrO_2; <0.6 methoxy molecules per V atom for vanadia on CeO_2), which is consistent with the simplified isotherm assumed in the kinetic derivation by Holstein and Machiels [16].

Fig. 8(a) also shows that, for a given temperature, the steady-state concentrations of surface methoxy intermediates exhibit the same support effect as was observed in fixed bed TOFs (V_2O_5/CeO_2> V_2O_5/ZrO_2> V_2O_5/TiO_2>V_2O_5/Al_2O_3) [6,8,9]. This implies that methanol dissociative adsorption to surface methoxy intermediates has a significant influence on the overall TOF, although better quantification of this trend will require corrections for mass transfer effects. The data on catalytic activity, obtained by mass spectrometry, are presented in Fig. 8(b) and (c). The results in Fig. 8(b) indicate that below 250°C the methanol conversion is less than about 30%, and under these conditions the selectivity to formaldehyde remains quite high [6,8,9]. Also, use of 5% Pt/Al_2O_3 at 300°C in the IR cell resulted in 100% methanol conversion, indicating that measured conversions are not affected by reactant gas bypass. The TOFs in the IR cell were calculated for the flow rate employed by normalizing these conversions to the number of active sites (surface V atoms). These apparent TOF values, shown in Fig. 8(c), are highest for 3% V_2O_5/CeO_2 and 4% V_2O_5/ZrO_2, followed by 5% V_2O_5/TiO_2, and were lowest for 25% V_2O_5/Al_2O_3.

4. Discussion

The complete quantitation desired from this data for the individual reaction steps requires the development of a mathematical reactor model to account for gas phase and intraparticle mass transport effects in the IR cell. Specifically, the activation energies calculated from the overall TOFs in Fig. 8(c) are ∼10 kcal mol^{-1}. Therefore, mass transfer effects are falsifying the kinetic data obtained from the IR cell, since the measured activation energies obtained from plug flow reactor (PFR) data for these catalysts are ∼20 kcal mol^{-1}. This is not very surprising, considering that there is no positive seal between the compressed wafer and the cell wall to prevent gas flow around the wafer (the cell design minimized dead space, but could not eliminate flow around the wafer). In fact, if there were no gas flow around the wafer it is likely that the wafers would have cracked due to the pressure drop induced by the flow, which is primarily normal to the wafer surface. However, this flow around the wafer is not actually bypass of the reactant gas as 100% conversion is possible (with 5% Pt/Al_2O_3). This means that enough contact time exists between the methanol gas and the catalyst for full conversion (i.e., no bypassing), but that the mass transfer driving force

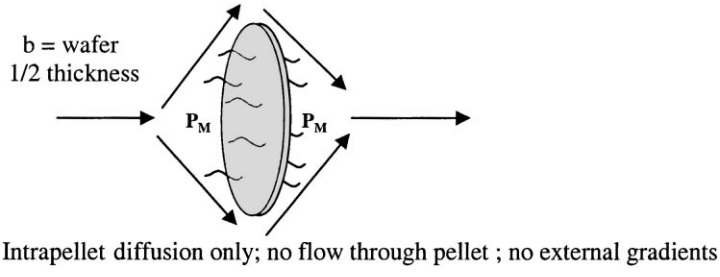

Fig. 9. Schematics of the reactor model.

is diffusion into the wafer rather than convective flow through it (which would require a positive seal around the wafer).

In an effort to model these effects, a preliminary reactor model has been developed according to the system depicted in Fig. 9. This model makes the following assumptions: (1) mass transport within the catalyst occurs only by intraparticle diffusion (unlike a PFR, there is no forced convection); (2) the surface methanol concentration in the gas phase is the known bulk concentration (no external, gas-phase gradients); and (3) diffusional mass transfer is only in the direction normal to the surface. This model is actually more appropriate for flow parallel to the wafer surface, but it will have to suffice as a first approximation in light of the fact that the present cell is clearly not behaving as a fixed-bed. The non-ideal flow patterns created by flow normal to the flat wafer surface prevent modeling of forced convective flow through the wafer or of any external gradients. Mathematically, the model involves solving a second-order, boundary value ordinary differential equation (ODE) for the concentration profile inside the catalyst wafer. The details of these equations are described in Appendix A. The ODE is linear if Eq. (8) is used to describe the reaction kinetics, but it is non-linear if Eq. (7) is used to account for water inhibition.

For the linear case, $\mathrm{TOF} = k_{\mathrm{overall}} \times C_{\mathrm{CH_3OH}}$, a well-known analytical solution exists [25] (see Appendix A). For the non-linear case, $\mathrm{TOF} = k_{\mathrm{overall}} \times C_{\mathrm{CH_3OH}}(C_{\mathrm{H_2O}})^{-1/2}$, a MATLAB® algorithm was written to numerically solve the problem using the 'shooting' method described by Conte [26]. Determination of the effective diffusion coefficient, D_e, was also required for the calculations. Calculations were performed using the gas-phase diffusivity of methanol in one case, and in another case using the D_e values ($\sim$0.01 $\mathrm{cm^2\ s^{-1}}$) calculated from the random pore model of Wakao and Smith [27]. For the latter case, the pore size distributions required for the random pore model were determined from nitrogen adsorption isotherms (BET instrumentation) and the model of Dollimore and Heal [28]. The pore size distributions are given in Fig. 10.

The results of these calculations for the determination of k_{overall} were most realistic using the linear, methanol only reaction term and the gas-phase diffusivity. The incorporation of water into the reaction term always led to unrealistically low values of k_{overall} (relative to the published PFR values of k_{overall}). The use of calculated effective diffusivity, D_e, values instead of gas-phase values led to calculated surface methoxy intermediate concentrations that were unrealistically high ($\gg$1 methoxy per V atom). The gas-phase effective diffusivities can be realistically justified based on the similar microporosities and diffusional pathlengths of both 75 μm particles (no diffusion limitations in fixed bed experiments) and the very thin IR wafers ($\sim$100 μm thick with the same chemisorption behavior as the powder). However, the failure in obtaining realistic results with the non-linear, water reaction rate term is somewhat puzzling. This may be related to the singularity at zero water concentration that exists in Eq. (7), suggesting that this empirical expression may not be valid for very low (absolute) water concentrations (methanol conversion to CH_2O and water approaches 50% in the IR experiments, but the absolute concentrations of methanol and water remain very low at <1%). Also, the apparent activation energy, $E_{\mathrm{app}} = E_a + \Delta H_{\mathrm{ads}}$, is expected to be somewhat lower for the IR experiments than for the fixed-bed experiments as ΔH_{ads} (a negative quantity) decreases in magnitude with increasing methanol

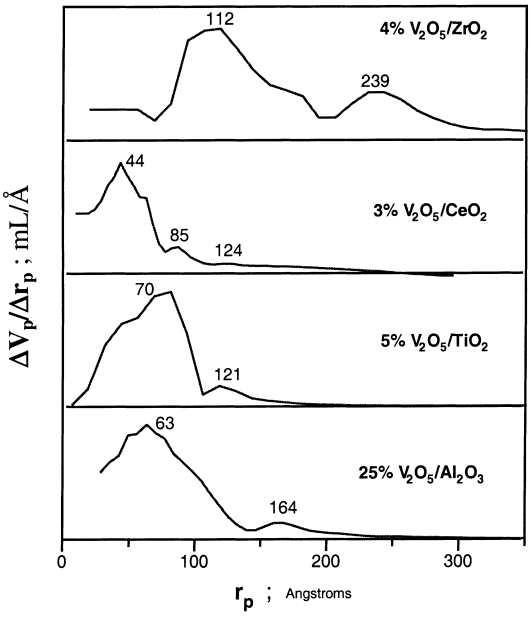

Fig. 10. Pore size distributions used for estimation of D_e (based on N_2 adsorption isotherms).

partial pressure and the IR and fixed-bed experiments were performed at 1% and 6% methanol, respectively. At present, however, even the best model results produce overall activation energies of only about 15 kcal mol^{-1} – values which are probably too low (compared to 20 kcal mol^{-1} from fixed-bed experiments) and indicate that mass transfer effects need to be modeled better for determination of $k_{overall}$.

It is possible to extract the desired values for the adsorption and surface decomposition constants, K_{ads} and k_{rds}, respectively, using the IR-observed methoxy intermediate concentrations once the values of $k_{overall}$ and their corresponding concentration profiles are known (see Appendix A for the equations). Calculations of these individual reaction step constants were performed using several different parameters as input: gas-phase D_e, calculated D_e, calculated values for $k_{overall}$, and published PFR values for $k_{overall}$ due to the different assumptions which can be made regarding D_e and $k_{overall}$. The most realistic results ($\theta_{OCH_3,\,surf.} < 1$ OCH_3 molecule per V atom; and $E_{a,rds} = \sim 25$ kcal mol^{-1}) were obtained using the linear, methanol-only model with gas-phase D_e values and published PFR values for $k_{overall}$. Use of calculated D_e values led to unrealistically high $\theta_{OCH_3,\,surf.}$ values ($\gg 1$ surface methoxy intermediate per V atom), as was the case in the calculation of $k_{overall}$. The use of the calculated values of $k_{overall}$, for either calculated or gas-phase D_e parameters, always led to unrealistically low activation energies for the surface decomposition rate constant, k_{rds} ($E_{a,rds}$<20 kcal mol^{-1}). These low activation energies are not surprising, since $k_{rds} = k_{overall}/K_{ads}$ (see Appendix A) and the calculated E_{app} values corresponding to $k_{overall}$ were always undercalculated by the model, relative to the published PFR values.

Using the best results (gas-phase D_e, $k_{overall}$ from published PFR data, and methanol-only reaction rate term) it is possible to compare the magnitudes of the individual adsorption and surface decomposition steps across all tested catalysts. Such a comparison is given in Fig. 11 for catalysts run at 225°C (note that the scale is relative to the highest value of each parameter to aid in comparison). This figure shows that both the adsorption equilibrium constant, K_{ads}, and the surface decomposition constant, k_{rds}, increase with the PFR TOFs for the series $V_2O_5/(Al_2O_3 < TiO_2 < ZrO_2 < CeO_2)$. Specifically, K_{ads} shows a $\sim$ six times increase

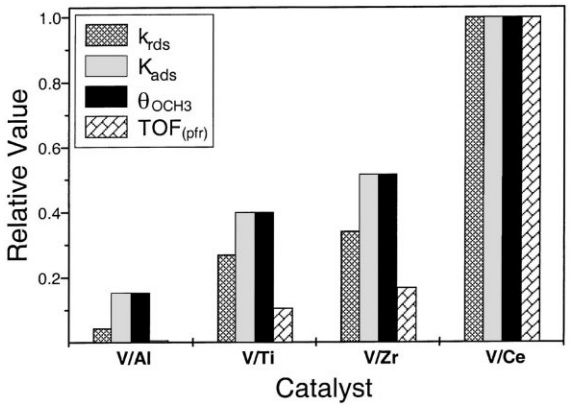

Fig. 11. Relative changes in the kinetic parameters as a function of the catalyst support at 225°C.

for this series of catalysts, whereas k_{rds} shows a $\sim$ 22 times increase in value. Thus, changes in both the adsorption equilibrium and the surface decomposition properties of supported metal oxide catalysts appear to be responsible for the support effect, although the methoxy decomposition is clearly the reaction step that is more sensitive to the specific metal oxide support.

Fundamentally, it has been proposed that these adsorption and surface decomposition steps correlate with the electronegativity of the support cation [8,9]. Adsorption of slightly acidic methanol will occur more readily on V–O-support bonds with higher basicity – this requires a more electropositive support cation to concentrate electron density on the bridging oxygen. The subsequent methoxy decomposition to formaldehyde is believed to occur via hydride abstraction of a methoxy methyl hydrogen by the support cation, a process which is again dependent upon the density of accessible electronic states in the support cation [8,9]. The present study supports these proposed ideas, since both K_{ads} and k_{rds} generally increase with decreasing electronegativity of the support cation (Sanderson electronegativity decreasing as follows: Al > Ti, Zr > Ce [8,9]). The origin of the support effect, therefore, appears to be the electronegativity of the support cation, which influences both the rate of methoxy decomposition through hydride abstraction and the steady-state equilibrium adsorption capacity of methanol to surface methoxy intermediates through the basicity of the bridging V–O-support bond (the adsorption site).

Table 1
Summary of heats of adsorption, activation energies, and preexponential factors[a]

	$\theta_{OCH_3} = A_{ads}\exp(+\lvert\Delta H\rvert/RT)P_{CH_3OH}$		$TOF = A\exp(-E_a/RT)\theta_{OCH_3}$		$E_{app} = E_a + \Delta H_{ads}$ (kcal mol^{-1})
	ΔH_{ads} (kcal mol^{-1})	A_{ads}	E_a (kcal mol^{-1})	A	
25% V_2O_5/Al_2O_3	−4.80	6.85×10^{-5}	24.8	1.07×10^{9}	20.0
5% V_2O_5/TiO_2	−8.71	3.44×10^{-6}	30.7	2.53×10^{12}	22.0
3% V_2O_5/CeO_2	−5.91	1.43×10^{-4}	25.9	7.50×10^{10}	20.0
4% V_2O_5/ZrO_2	−3.54	9.27×10^{-4}	21.5	2.66×10^{8}	18.0

[a] Units: θ_{OCH_3} – methoxy molecules/V atom; A_{ads} – methoxy molecules/(V atom Torr MeOH); TOF – methanol molecules converted/(V atom s); A – s^{-1}.
Note also that 1 methanol molecule = 1 methoxy molecule.

Some additional evidence suggests that these calculated constants, K_{ads} and k_{rds}, are reasonably good estimates of their true values. Firstly, thermodynamic values calculated from the temperature dependencies of these constants (see Table 1 for ΔH_{ads} and E_a values; Table 2 for $\Delta S^{\ddagger}$ of the transition state [29]) indicate that E_a for the surface reaction is ∼25–30 kcal mol^{-1}, while ΔH_{ads} is ∼ −5 to −10 kcal mol^{-1}. These values are generally expected for adsorption and reaction of methanol on oxide catalysts [16].

Secondly, when the catalysts were run under the same conditions as in the original experiments, but in a different cell (Harrick Scientific HTC-100) which was certain to have no convective flow through the wafer, similar values for surface methoxy concentrations were obtained. This means that the original experiments were close to the diffusion-based transport regime used in the mathematical model, and that the observed surface methoxy concentrations are somewhat insensitive to the actual deviations from the idealized reactor model which are present in the real cell. This insensitivity is also consistent with the fact that calculated concentration gradients in the thin IR wafers were generally small (<10% decrease at the centerline of the wafer, relative to the surface concentration). The use of the reactor model to calculate the overall rate constant, $k_{overall}$, from the mass spectrometer data appears to be much more sensitive to experimental and model error. However, since $k_{overall}$ is an intrinsic kinetic parameter independent of reactor configuration, the more reliable fixed bed values may be used in the diffusion-based reactor model of the IR cell to correct the measured methoxy concentrations for mass transfer effects.

Table 2
Summary of entropies of transition[a]

$A = (kT/h) \times \exp(\Delta S^{\ddagger}/R)$	
Catalyst	$\Delta S^{\ddagger}$ at 498 K (kcal mol^{-1})
25% V_2O_5/Al_2O_3	−0.018
5% V_2O_5/TiO_2	−0.0028
3% V_2O_5/CeO_2	−0.0098
4% V_2O_5/ZrO_2	−0.021

[a] Note: k – Boltzmann constant; h – Planck constant; R – gas constant.

5. Conclusions

The mechanistic origin (adsorption equilibrium, rate-determining methoxy surface decomposition, or desorption equilibrium) of the support effect was investigated using in situ IR spectroscopy of supported vanadia catalysts during methanol oxidation. Specifically, the steady-state surface concentrations of adsorbed surface methoxy intermediates on monolayer catalysts (∼8 V atoms nm^{-2}) of V_2O_5/(TiO_2, CeO_2, Al_2O_3, and ZrO_2) were measured with in situ infrared spectroscopy/mass spectrometry. The IR extinction coefficient of these surface methoxy species (2830 cm^{-1} band) was determined from vacuum dosing experiments to be 13.3 cm^{-1} per μmole of methoxy molecules per gram of catalyst (for a 50 mg wafer). For all tested catalysts, at a given temperature, the steady-state concentration of surface methoxy intermediates was higher for the catalysts with the higher fixed bed TOFs ($V_2O_5/CeO_2 > V_2O_5/ZrO_2 > V_2O_5/TiO_2 > V_2O_5/Al_2O_3$). This implies that metha-

nol dissociative chemisorption to surface methoxy intermediates has significant influence on the overall TOF. Also, for the V_2O_5/CeO_2 catalyst, the V=O fundamental stretching vibrations at $\sim$1029 cm^{-1} exhibit only a 24% decrease in intensity at 300°C during in situ methanol oxidation, relative to the fully oxidized intensity. Hence, the catalyst is primarily in the V^{+5} fully-oxidized state during methanol oxidation (a conclusion also supported by recent in situ UV–Vis DRS experiments).

Corrections for mass transfer in the catalyst wafers used in the transmission IR studies involved analytical and numerical solutions to the second-order, boundary value ordinary differential equations that constitute the mass balances for the system. The best results were obtained using gas-phase effective diffusivities and the methanol-only (no water term) reaction rate expression. However, corrected overall activation energies were still unrealistically low ($\sim$15 kcal mol^{-1}) and indicate that mass transfer effects have not been completely incorporated into the model. Estimates of the individual adsorption equilibrium and surface decomposition rate constants (as well as the fundamental thermodynamic properties ΔH_{ads}, E_a and $\Delta S^{\ddagger}$) could still be made by using published fixed bed rate constants in conjunction with the new IR data as sets of reliable data for the model because the surface methoxy concentrations were much less sensitive to model deviations than were the rate constants. The results indicated that E_a for the surface reaction is 25–30 kcal mol^{-1}, while ΔH_{ads} is -5 to -10 kcal mol^{-1} – values that are generally expected for adsorption and reaction of methanol on oxide catalysts.

More importantly, the adsorption equilibrium constant, K_{ads}, showed a $\sim$ six times increase for vanadia on oxide supports of Al < Ti < Zr < Ce, whereas the surface decomposition rate constant, k_{rds}, showed a $\sim$ 22 times increase in value over these same catalysts. Thus, changes in both the adsorption equilibrium and the methoxy decomposition properties of supported metal oxide catalysts appear to be responsible for the support effect, although the methoxy decomposition is clearly the reaction step that is more sensitive to the specific metal oxide support. In addition, the more fundamental origin of the support effect appears to be the electronegativity of the support cation, which influences both the rate of methoxy decomposition through hydride abstraction and the steady-state equilibrium adsorption capacity of methanol to surface methoxy intermediates through the basicity of the bridging V–O-support bond (the adsorption site).

6. Nomenclature

b	wafer 1/2 thickness (cm)
C_A	concentration of methanol (mol/cm^{-3})
C_{A0}	surface concentration of methanol (mol cm^{-3})
D_e	effective diffusivity of methanol (cm^2 s^{-1})
E_a, ΔH_{ads}, $\Delta S^{\ddagger}$	activation energy, heat of adsorption, entropy of transition (kcal mol^{-1})
F_A	molar flowrate of methanol (mol s^{-1})
K_{ads}	adsorption equilibrium constant (methoxy molecules/(V atom Torr MeOH))
k_{rds}	rate-determining step kinetic constant (s^{-1})
$k_{overall}$	overall rate constant (methanol molecules/(V atom s Torr MeOH)) {converted to: cm^3 of methanol/(gcat s) for use in mass balance}
P_{CH_3OH}	$C_A \times RT$ = partial pressure of methanol (Torr)
r	wafer radius (cm)
TOF	turn-over frequency (methanol molecules converted/(V atom s))
W_A	molar flowrate of methanol across wafer surfaces (mol s^{-1})
x_A	$(C_{A0}-C_A)/C_{A0}$ = conversion of methanol (dimensionless)
z	flow direction (cm)
η	effectiveness factor (dimensionless)
θ_{OCH_3}	coverage of methoxy molecules (methoxy molecules/V atom)
ρ_s	wafer bulk density (gcat cm^{-3})

Acknowledgements

The authors gratefully acknowledge the United States Department of Energy – Basic Energy Sciences (Grant #DEFG02-93ER14350) for financial support of this work.

Appendix A

Model equations

The intraparticle mass balance is as follows for the linear, methanol-only reaction term – A = methanol, z = flow direction (normal to wafer surface), b = wafer 1/2 thickness, ρ_s = wafer bulk density:

$$D_e \frac{d^2 C_A}{dz^2} - k_{overall} \rho_s C_A = 0 \quad (A.1)$$

$$\text{B.C}: \quad (1) C_A = C_{A0} \quad \text{at} \quad z = b$$

$$\text{B.C}: \quad (2) \frac{dC_A}{dz} = 0 \quad \text{at} \quad z = 0$$

Provided that all parameters are known, including $k_{overall}$ – the apparent rate constant, the above equation may be solved to give the concentration profiles of methanol within the wafer. These concentration profiles are then related to the surface methoxy intermediate concentrations, as determined from the IR spectra, as follows: (Note that the following equations are for the linear, methanol-only reaction rate term, but the water term can be included by dividing P_{CH_3OH} by $(P_{H_2O})^{0.5}$).

Measured quantity (from IR) is average methoxy concentration:

$$\bar{\theta}_{OCH_3} = \frac{2\int_0^b \theta \, dz}{2b} \quad (A.2)$$

Adsorption equilibrium (at low coverage)

$$\theta_{OCH_3} = K_{ads} P_{CH_3OH} \quad (A.3)$$

Integrate over wafer thickness:

$$2\int_0^b \theta \, dz = 2K_{ads} \int_0^b P_{CH_3OH} \, dz \quad (A.4)$$

The desired equilibrium and rate constants for the individual steps of adsorption and surface decomposition, respectively, are as follows:

Adsorption step

$$K_{ads} = \frac{b\bar{\theta}_{OCH_3}}{\int_0^b P_{CH_3OH} \, dz} \quad (A.5)$$

Surface decomposition step:

$$k_{rds} = \frac{k_{overall}}{K_{ads}} \quad (A.6)$$

For the experiments to be internally consistent and to test the validity of the model, $k_{overall}$ can also be calculated directly from the overall mass balance to check how close the values are to the PFR data (F_A = molar flowrate; x_A = conversion; r = wafer radius):

$$\text{overall mass balance}: \quad 0 = F_{A,in} - F_{A,out} + |W_A| \quad (A.7)$$

where

$$|W_A| = 2\pi r^2 D_e C_{A0} (dx_A/dz)_{z=b}$$

Appendix

Methods of solution

Linear, first-order, methanol-only kinetics:

Analytical solution to wafer mass balance [25]:

1. Concentration (partial pressure) profile:

$$P_{CH_3OH} = P^{surface}_{CH_3OH} \frac{\cosh\left(z\sqrt{k_{overall}\rho_s/D_e}\right)}{\cosh\left(b\sqrt{k_{overall}\rho_s/D_e}\right)} \quad (B.8)$$

2. Pressure integral over wafer half-thickness, b (from integral tables):

$$\int_0^b P_{CH_3OH} \, dz = \frac{P^{surface}_{CH_3OH}}{\cosh\left(b\sqrt{k_{overall}\rho_s/D_e}\right)} \cdot \left[\frac{1}{\sqrt{k_{overall}\rho_s/D_e}}\left(\sinh\left[b\sqrt{\frac{k_{overall}\rho_s}{D_e}}\right] - \sinh(0)\right)\right] \quad (B.9)$$

3. Effectiveness factor for the wafer:

$$\eta = \frac{TOF_{IR}}{TOF_{PFR}} = \frac{TOF_{IR}}{k_{overall} P_{CH_3OH}} = \frac{\tanh\left(b\sqrt{k_{overall}\rho_s/D_e}\right)}{\left(b\sqrt{k_{overall}\rho_s/D_e}\right)} \quad (B.10)$$

4. Note that η may be used to write a different, but equivalent, form of the overall mass balance:

$$TOF_{IR} = TOF_{PFR} \times \eta \quad (B.11)$$

References

[1] H.R. Gerberich, G.C. Seaman, Formaldehyde, Kirk-Othmer Encyclopedia of Chemical Technology, 4th ed., vol. 11, Wiley, New York, 1994, pp. 929–951.
[2] J.M. Tatibouët, Appl. Catal. A 148 (1997) 213.
[3] I.E. Wachs, G. Deo, M.A. Vuurman, H. Hu, D.S. Kim, J.M. Jehng, J. Mol. Catal. 82 (1993) 443.
[4] F. Roozeboom, P.D. Cordingley, P.J. Gellings, J. Catal. 68 (1981) 464.
[5] P. Forzatti, E. Tronconi, A.S. Elmi, G. Busca, Appl. Catal. A 157 (1997) 387.
[6] G. Deo, I.E. Wachs, J. Catal. 146 (1994) 323.
[7] I.E. Wachs, G. Deo, J.M. Jehng, D.S. Kim, H. Hu, in: B.K. Warren, S.T. Oyama (Eds.), Heterogeneous Hydrocarbon Oxidation (ACS Symposium Series 638), ACS Press, Washington, 1996, pp. 292–299.
[8] I.E. Wachs, G. Deo, M.V. Juskelis, B.M. Weckhuysen, in: G.F. Froment, K.C. Waugh (Eds.), Dynamics of Surfaces and Reaction Kinetics in Heterogeneous Catalysis, Elsevier, Amsterdam, 1997, pp. 305–314.
[9] I.E. Wachs, in: J.J. Spivey (Ed.), Catalysis, vol. 13, The Royal Society of Chemistry, Cambridge, 1997, pp. 37–54.
[10] H. Hu, I.E. Wachs, J. Phys. Chem. 99 (1995) 10911.
[11] D.S. Kim, I.E. Wachs, K. Segawa, J. Catal. 146 (1994) 268.
[12] G. Busca, J. Mol. Catal. 50 (1989) 241.
[13] A. Elmi, E. Tronconi, C. Cristiana, J.G. Martin, P. Forzatti, G. Busca, Ind. Eng. Chem. Res. 28 (1989) 387.
[14] G. Busca, A. Elmi, P. Forzatti, J. Phys. Chem. 91 (1987) 5263.
[15] X. Gao, I.E. Wachs, unpublished results, 1998.
[16] W. Holstein, C. Machiels, J. Catal. 162 (1996) 118.
[17] E. Santacesaria, M. Morbidelli, S. Carra, Chem. Eng. Sci. 36 (1981) 909.
[18] P. Jiru, J. Tichy, B. Wichterlova, Coll. Czech. Chem. Commun. 31 (1966) 674.
[19] R.S. Mann, M.K. Dosi, J. Catal. 28 (1973) 282.
[20] W. Farneth, L. Briand, I.E. Wachs, unpublished results, 1998.
[21] M.A. Vuurman, D.J. Stufkens, A. Oskam, G. Deo, I.E. Wachs, J. Chem. Soc., Faraday Trans. 92 (1996) 3259.
[22] J.M. Jehng, G. Deo, B.M. Weckhuysen, I.E. Wachs, J. Mol. Catal. A 110 (1996) 41.
[23] C.A. Emeis, J. Catal. 141 (1993) 347.
[24] L. Briand, I.E. Wachs, unpublished results, 1998.
[25] R.B. Bird, W.E. Stewart, E.N. Lightfoot, Transport Phenomenon, Wiley, New York, 1960.
[26] S.D. Conte, Elementary Numerical Analysis: An Algorithmic Approach, McGraw-Hill, New York, 1965, pp. 268–269.
[27] N. Wakao, J.M. Smith, Chem. Eng. Sci. 17 (1962) 825.
[28] D. Dollimore, G.R. Heal, J. Appl. Chem. 14 (1964) 109.
[29] S. Glasstone, K.J. Laidler, H. Eyring, The Theory of Rate Processes: The Kinetics of Chemical Reactions, Viscosity, Diffusion and Electrochemical Phenomena, McGraw-Hill, New York, 1941, pp. 195–201.